Center for Optical Technologies
Biophotonics Group Research Activities, 2010

Synthesis and optical detection of HIV pseudo viruses: Cassi R Wentz, Cassie Phillips, Xuanhong Cheng and H. Daniel Ou-Yang (hdo0@lehigh.edu), *Lehigh University*. We aim to directly enumerate whole viral particles in blood. In the unprocessed state, however the viral load is often well below the detection thresholds of even the most sensitive optical techniques. Recently we have shown that optical trapping can be used to locally concentrate synthetic nanoparticle suspensions in the detection region, making optical detection of whole viral particles possible in the biological sample. In order to create a surrogate bio-nanoparticle suspension for this ongoing work, we synthesized non-replicating pseudo HIV particles using plasmids carrying the essential HIV genes. A protein found on the core of the HIV virus, (gag) was genetically engineered to carry a green fluorescent tag, and we showed that Fluorescent Correlation Spectroscopy can be used to quantify aggregates of this protein in solution in the same manner as synthetic nanoparticles. Future work will extend this hybrid optical method to the quantification of whole pseudo viral particles expressing the gag-GFP tag.

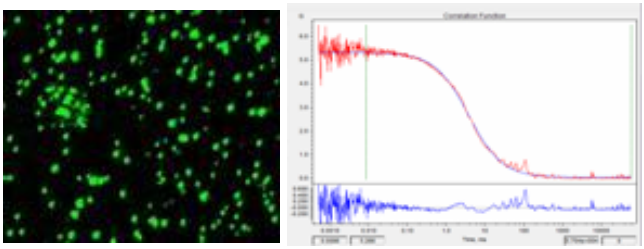

Fig. (Left) Fluorescently labeled protein aggregates (Gag GFP) when viewed under confocal microscope. (Right) FCS correlation curve recorded from gag GFP protein in solution. The amplitude of the curve can be used to deduce the number density of proteins in the detection volume.

Improving fluorescence imaging of biological cells on biomedical polymers: Israd H. Jaafar, Courtney E. LeBlon, Ming-Tzo Wei, Daniel Ou-Yang, John P. Coulter, Sabrina S. Jedlicka (ssj207@lehigh.edu) *Lehigh University*. Traditional fluorescence based cell imaging is often a challenge on polymeric biomaterials. Some polymeric biomaterials are highly auto-fluorescent, which overcomes any fluorescent protein marker that may be used. One polymer of this type is poly(glycerol sebacate) (PGS), which has many potential uses in bioengineering. Many of the current works that encounter polymer auto-fluorescence or light scattering will replace traditional fluorescence based immunocyto-chemistry protein analysis for more time intensive or expensive techniques. To address the problem of auto-fluorescence and light scattering phenomena in biomaterial polymers, we used Sudan Black Dye B (SB) to quench auto-fluorescence and light scattering in biomedically relevant polymers. We believe that the SB quenching phenomenon is a result of the SB high light absorption capacity, where the SB is simply absorbing photons emitted and scattered by the polymeric structures.

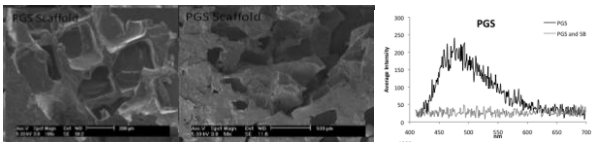

Fig. SEM of polymers (a) before and (b) after SB treatment; (c) fluorescence spectrum of polymers with and without SB

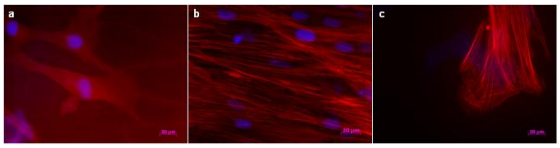

Fig. Fluorecent images of cells cultured on the polymers and stained for actin (red) and nuclei (blue). (a) hMSCs on PGS before SB (b) hMSCs on PGS after SB (c) hMSCs on glass coverslips for comparison.

Thermal and non-thermal fluctuations of the mechanical properties in living cells: Ming-Tzo Wei and H. Daniel Ou-Yang (hdo0@lehigh.edu), *Lehigh University*. Intracellular stresses generated by molecular motors can actively modify the cytoskeletal network, causing changes in intracellular mechanical properties; prompting us to study the out-of-equilibrium microrheology in living cells. This work reports measurements of the intracellular mechanical properties using both passive and active microrheology approaches using endogenous organelle particles as probes. Using the fluctuation-dissipation theorem, we compared the two approaches to distinguish thermal and non-thermal fluctuations of mechanical properties in living cells. The differences between the experimental results by passive and active approaches indicate that there were active driving forces (e.g., motor activities) that influenced the microenvironment surrounding the probes.

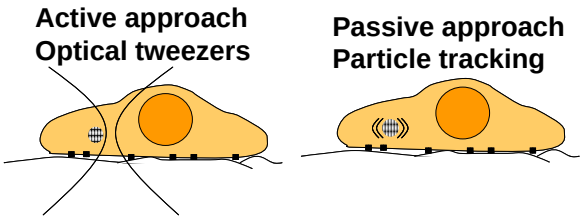

Fig. Sketch of the two cellular microrheology techniques. The left figure shows the active approach in which an oscillatory optical tweezers is used to manipulate an endogenous intracellular organelle. The right figure shows the passive approach where a CCD camera is used to track fluctuations in the particle position.

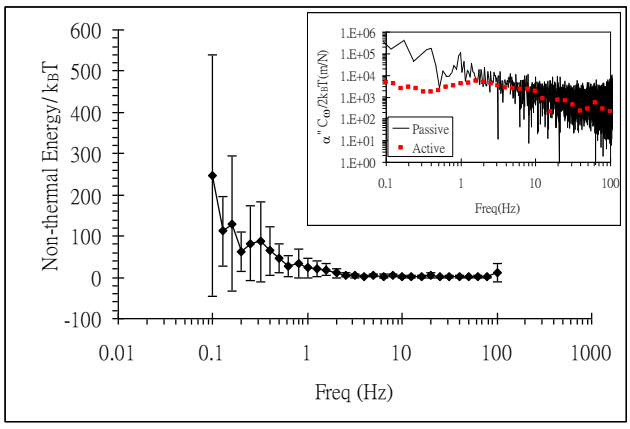

Fig. Experimental results of $E_{non\text{-}thermal}/k_BT$, the ratio of the non-thermal energy to the thermal energy as a function of frequency. (Right) The imaginary part of the compliance (α") determined by active microrheology (*dots*) and the normalized power spectrum $\omega C(\omega)/2k_BT$ measured by passive microrheology (*lines*).

Response of mitotic HeLa cells to mechanical perturbations: Ming-Tzo Wei, Dimitrios Vavylonis, and H. Daniel Ou-Yang (hdo0@lehigh.edu), *Lehigh University*. The cortical actomyosin layer below the membrane of dividing cells and the astral microtubules of the mitotic spindle are coupled through internal feedback mechanisms that regulate the local and global mechanical properties of the cell. We conducted an experiment to perturb mitotic Hela cells with controlled and localized forces while following the cellular response using fluorescence imaging. Anti-integrin coated micro-beads were attached to HeLa cells expressing MRLC-GFP. We applied external forces to a bead by an optical tweezers and imaged the dynamics of myosin-II and mitotic spindle during cell division. Experimental results showed that the mitotic spindle appeared to move to an asymmetric post perturbation position. This observation is consistent with the expected coupling between force-dependent cortical flow and spindle position and will be useful in more detailed studies of the response of cytoskeleton to external or internal forces.

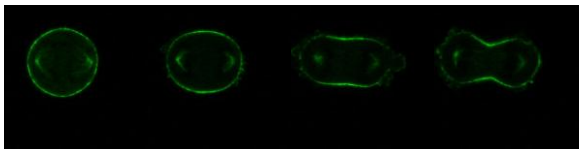

Fig. Images of dividing cells expressing myosin regulatory light chain fused to GFP (MRLC-GFP). Single confocal slices obtained at 900 sec intervals. The images show increasing concentration of myosin into an equatorial region during anaphase and cytokinesis. MRLC labels (non-specifically) the pole of the mitotic spindle; this enabled us to visualize the assembly of myosin in the equatorial region simultaneously with the position of the mitotic spindle.

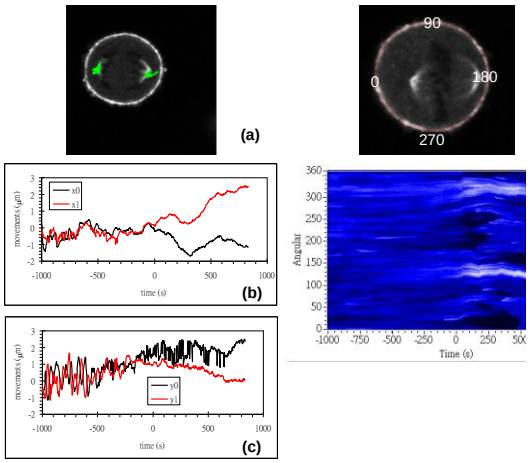

Fig. Simultaneous tracking of the position of the spindle poles and cortical myosin distribution. (a) Software for

particle tracking was used to locate the position of the spindle poles. (b) Graph of the horizontal displacement of the spindle poles. Time *t*=0 is the onset of anaphase B at which time the spindle poles start to move away from one another. (c) Vertical displacement of spindle poles. Periodic oscillatory behavior was observed at times -1000 through -500 sec. (d) Active contours that adapt to the cell boundary were used to monitor the intensity of MRLC along the cell's cortex. (e) Kymograph of myosin concentration as a function of angle and time (bright = higher intensity). Myosin starts to assemble in a contractile ring corresponding to two bight bands during anaphase. The image shows the same cell as in (b) and (c). The dark regions are blebs that develop during cytokinesis as the cortex of the cell weakens along the flanking regions.

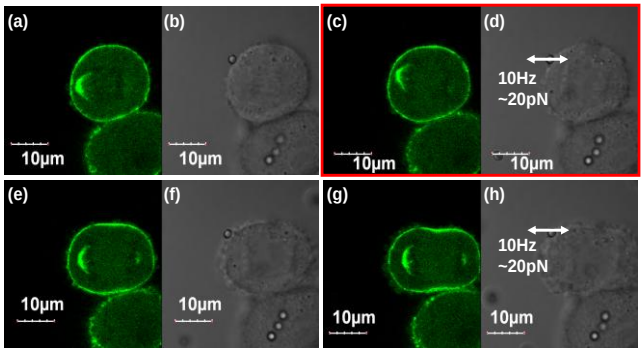

Fig. Fluorescence and DIC images showing the effect of mechanical perturbations of Hela cells expressing MRLC-GFP. The images show a cell proceeding through anaphase and cytokinesis. A bead is attached to cell membrane. (a) and (b) show a cell prior to an external force. (c) and (d) show the effect of an oscillatory force on the bead: the pole moved towards the bead. In (e) and (f) no external force was applied and the pole returns to a symmetric position. In (g) and (h), i.e. during cytokinesis an external force has no observable effect.

Observe the active response of cell cytoskeleton reorganization to mechanical forces Pei-Wen Yen, Ming-Tzo Wei A. Chiou, and H. Daniel Ou-Yang (hdo0@lehigh.edu), *Lehigh University*. Mechanical forces are essential for cell homeostasis. When a mechanical force is applied to adherent cells, the cells reorganize the cytoskeleton and generate stress fibers to balance the mechanical force. If the mechanical force is not balanced by the cell, it will activate signal transduction pathways. In this study, we focused on the cellular response to mechanical forces under different polymerization states. We used GFP to label the cytoskeleton and confocal microscopy to observe the real time response of the cell reorganization under shear flow. We examined three different cytoskeleton polymerization states, normal cells (control), cells with polymerized actin (using transfected Tir plasmids), and cells with depolymerized cytoskeletons (by adding 0.5μM latrucullin A). For each experiment, we analyzed the formation of cell cytoskeleton stress fibers along a particular direction, noting the orientation angle between the cell's major axis and the stress fiber direction. We found that the different polymerization states led to diverse inner cytoskeleton distributions (inner stress forces), indicating different responses to maintain cellular homeostasis.

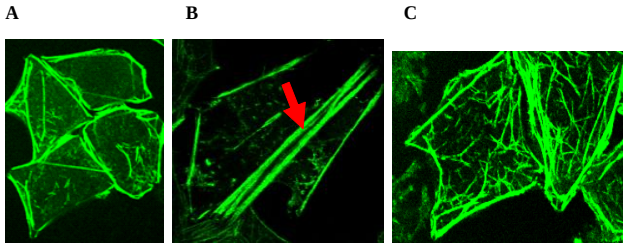

Fig. The three different cytoskeleton polymerization state cell (A) normal cell; (B) transfect Tir plasmid into cell to polymerize the acti; and (C)adding 0.5μM latrucullin A to depolymerize the cell cytoskeleton.

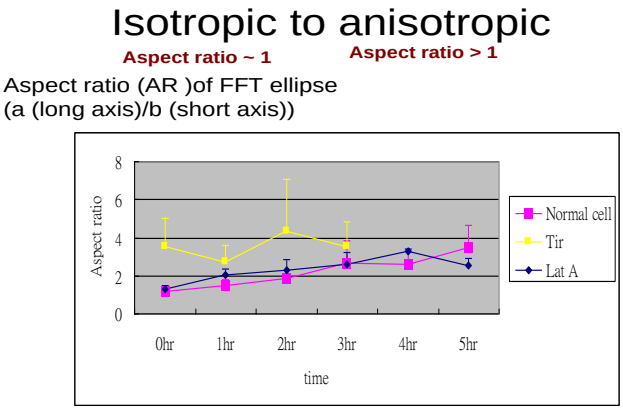

Fig. (A)The aspect ratio (long axis/short axis) of cells under shear stress. The different response to 3 different polymerization state cells under shear stress. From left to right: normalcell, Tir transfected cell, and Latrucullin A cell respectively.

Nanospectroscopy and imaging with non-Gaussian optical trapping/manipulation: Liangcheng Zhou Qiwen Zhan, Volkmar Dierolf, and Daniel Ou-Yang (hdo0@lehigh.edu), *Lehigh University*. We have developed an optical trapping system for *in situ* imaging and spectroscopy using non-Gaussian laser beams with radial or azimuthal polarizations. We

have demonstrated that trapping by radial polarized light creates an ideal situation for 3D trapping of spherical or anisotropic nanoparticles. Additionally, azimuthal polarization has also been explored in our lab, and has been shown to exhibit intriguing uses in aligning nanoparticles in different shapes. Using a unique Olympus dual up/down confocal microscope, we have: 1. confined and fluorescently image nanoparticles in 3-D; 2. independently controled the E-field direction of the optical trap; 3. manipulate particle dynamics in an non-Gaussian optical trap with radial/azimuthal polarizations.

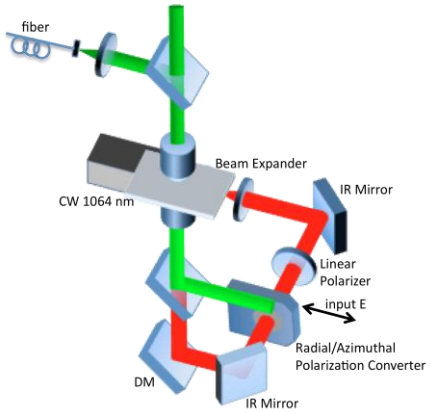

Fig. Schematics of the optical system for *in situ* trapping and imaging using non-Gaussian laser beams.

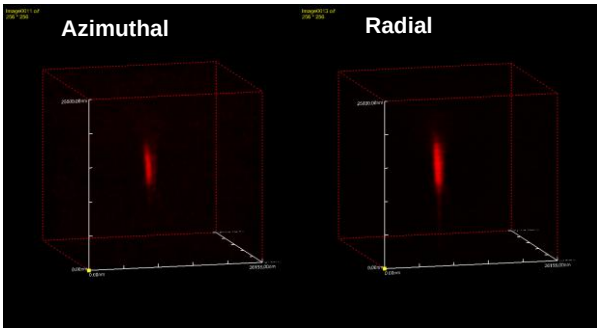

Fig. Polystyrene nanoparticles (size = 210nm) trapped with azimuthally and radial polarized light orient in different shapes .

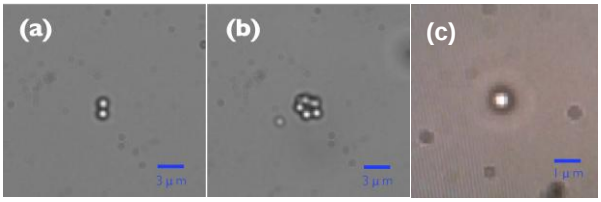

Fig. (a) (b)Polystyrene particles (size = 1 μm) trapped with azimuthally polarized light orient in different shapes . (c) Individual ZnO nanowire with aspect ratio of 10 trapped with radially polarized light.

Surface plasmon resonance for dynamic analysis of cell secretion behaviors: S-H. Wu, M-T. Wei, A. Chiou, P-K. Wei, and X. Cheng (xuc207@lehigh.edu), *Lehigh University*. The dynamics of protein secretion are fundamental to the understanding of many biological phenomena. However, measurement of temporal protein secretion is currently limited to destructive and low-throughput techniques, and often requires a large number of cells. To answer the demand for a label-free and high throughput platform to study cell secretor activities in real time, we designed an opto-fluidic system where acute human monocytic leukemia cells (THP1), were cultured in a microfluidic chip and their dynamic secretion of matrix metalloproeinase 9 (MMP9) was studied in situ using surface plasmon resonance (SPR). MMP9 is an enzyme for extra cellular matrix breakdown and is involved in the regulation of several cytokines and growth factors. It also plays an important role in many diseases, such as arthritis, metastasis and tumor-associated tissue remodeling. THP1 cells treated with LPS are known to secrete significant amount of MMP9, which is enriched in the microfluidic culture chip and detectable by the on-chip SPR sensor in real time without an additional label. SPR-based sensors detect refractive index changes within ~200 nm from the sensor surface with high sensitivity, thus becoming a popular choice for dynamic analysis of bio-molecular binding phenomena. Direct application of SPR to *in situ* detection of cell secretants presents a novel utility of SPR. In addition, our feasibility study demonstrates that our opto-fluidic system holds great potential for dynamic cell function analysis and drug screening in future research.

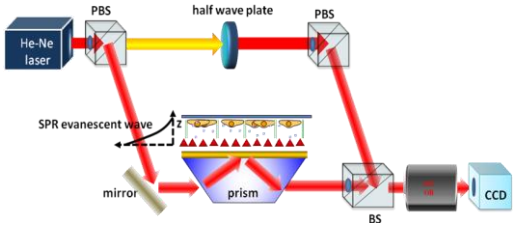

Fig. A schematic of surface plasmon resonance experimental system

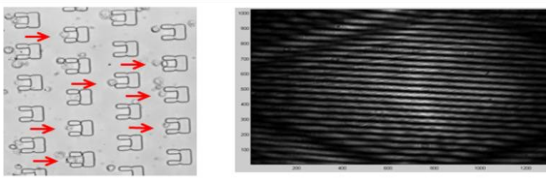

Fig. Cell trapping and SPR interference image

Plasmonic Mach-Zehnder Interferometer for compact and sensitive sensing applications: Q. Gan, Y. Gao and F. J. Bartoli (fjb205@lehigh.edu) *Lehigh University*. Plasmonic Mach-Zehnder Interferometer was proposed to perform miniaturized and sensitive surface plasmon resonance sensing. Plasmonic interferences arise from coherently coupled pairs of subwavelength slits, illuminated by a broadband optical source, and this interference modulates the intensity of the far-field scattering spectrum. Experimental results, obtained using a simple experimental setup, are presented to validate theoretically predicted interferences introduced by the surface plasmon modes on top and bottom surfaces of a metal film. By observing the wavelength shift of the peaks or valleys of the interference pattern, this highly compact device has the potential to achieve a very high sensitivity relative to other nanoplasmonic architectures reported.

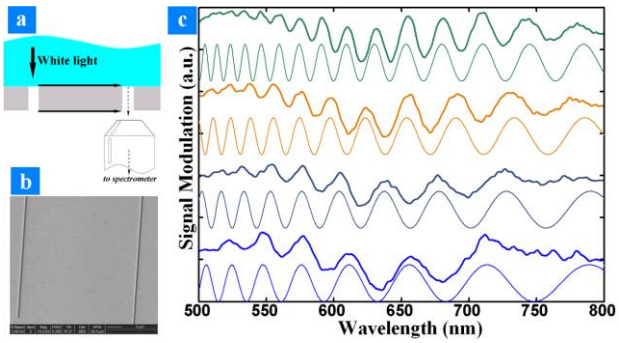

Fig. (a) Sketch of the doublet geometry. (b) A scanning electron microscope image of a doublet structure with a slit–slit separation distance of 15.73μm. (c) SPP-mediated spectral interference introduced by the SPP modes from the top and bottom surfaces: Here we study 4 doublet samples on a Ag film with slit–slit separation distances of 10.50μm (bottom), 13.12μm (lower center), 15.73μm (upper center) and 20.98μm (top). Bold solid lines are measurement results and the thin solid lines are theoretical predictions.

Nonlinear imaging of mitotic cancer cells: Wei Nie, Ivan Biaggio, H. Daniel Ou-Yang, and Dimitrios Vavylonis (vavylonis@lehigh.edu), *Lehigh University*. Myosin is a motor protein that plays an important role in the process of mitosis. During the cytokinesis stage, actin and myosin are assembled into filaments and form a contractile ring around the cell's equator. Myosin consists of two heavy chains, two heads and two light chains. The non-centrosymmetric structure of the heavy chains and heads in myosin produces strong nonlinear effects when illuminated with a high intensity laser, which makes it a good candidate for second harmonic imaging microscopy (SHIM). The experimental results shown include both a GFP (MRLC-GFP) image (red) and a SHG (green) image of a dying HeLa cell.

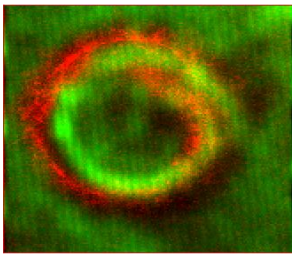

Fig A combined image of the fluorescence image labed in red, and the SHG inag labed in green.

Measurements of charged colloidal bulk moduli using optical bottles: Joseph Junio, and H. Daniel Ou-Yang (hdo0@lehigh.edu), *Lehigh University.* In a system of charge- stabilized colloids, the dominant force responsible for the interactions is due to the screened Coulomb repulsion. Forces between pairs of such charged surfaces have been extensively characterized using direct measurements from various configurations of optical tweezers. In lieu of trapping pairs of particles, we use the radiation pressure from a tightly focused laser to trap and concentrate ensembles of multiple particles. Fluorescence analysis of the trapped nanoparticles using a mechanical balance of radiation and osmotic pressures permits extraction of the trapping energy per individual nanoparticle, which is then used to compute the bulk modulus. Results of the osmotic bulk modulus as a function of solution ionic strength are presented and are compared to results from identical samples measured using turbidity spectra.

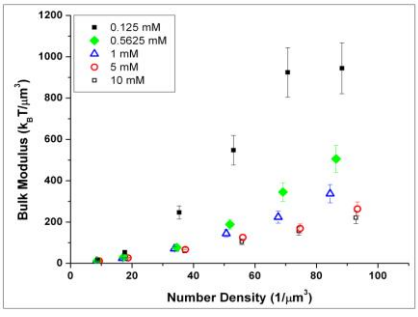

Fig. Osmotic bulk modulus measured by the *optical bottle* for samples of 100nm particles at different ionic strengths, plotted as a function of number density.

Fluorescence correlation spectroscopy in an optical trap: Yi Hu, Xuanhong Cheng and H. Daniel Ou-Yang (hdo0@lehigh.edu), *Lehigh University*. By focusing a laser beam into a suspension of particles, statistical analysis of the emitted fluorescence can be used to investigate the concentration and diffusion of fluorescent particles through fluorescence correlation spectroscopy (FCS). We ask how one might use FCS to investigate the behavior of nanoparticles in a tightly focused laser beam. Specifically, we ask 1) whether FCS can be used to enumerate the particles in the optical trap formed by the focused laser beam, 2) whether the trapping energy can be determined by analyzing the number of particles in the trap as a function of trapping laser intensity, and finally, 3) how fluorescence fluctuations change with the intensity of the trapping laser. This paper reports our findings from an experimental study to address these questions.

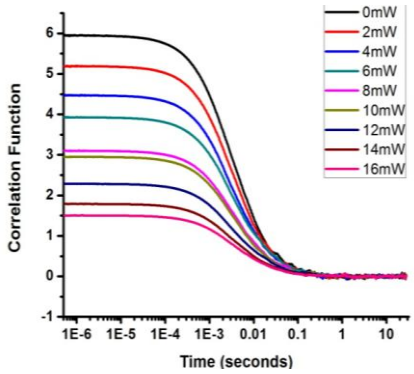

Fig. FCS autocorrelation functions for 0.01% suspensions of 100nm diameter nanoparticles under different trapping laser powers. Each curve represents an average of 10 measurements.

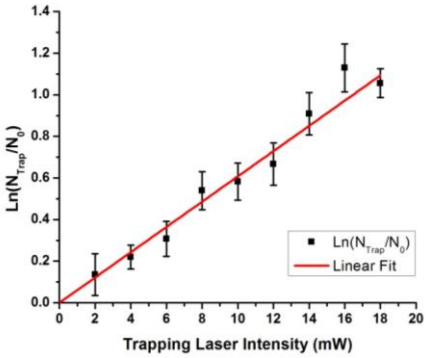

Fig. The enhancement of particle number in the observation volume shown in logarithmic scale versus the laser intensity. The number of particles in the trap increases exponentially with laser intensity, indicating that the particle number follows a Boltzmann-like distribution in the trapping energy. The slope of the graph can then be used to determine the trapping energy per particle.

Optical tweezers as a force sensor for separating dielectrophoresis and AC electroosmosis forces: Jingyu Wang and H. Daniel Ou-Yang (hdo0@lehigh.edu), *Lehigh University*. Forces experienced by colloidal particles in an AC electric field such as dielectrophoresis (DEP) and AC electro-osmosis (ACEO) have been widely investigated for applications in microfluidic devices. In order to provide a more complete theoretical basis for such AC electrokinetic mechanisms, we propose a method to quantify the two forces exerted on individual particles using optical tweezers as a force transducer with lock-in phase sensitive detection technique to allow high selectivity. Using this method, we isolated the ACEO force from the DEP force for charged polystyrene spheres in deionized (DI) water. ACEO-free DEP crossover frequencies and a comprehensive 2D-mapping of the frequency dependent ACEO forces are determined in this work.

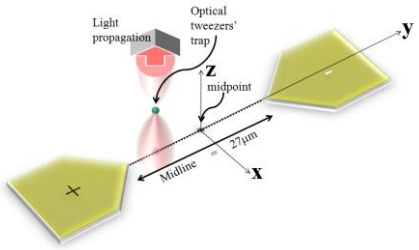

Fig. A schematic of the opposing microelectrodes design. The spacing between the electrodes was measured to be 27 μm.

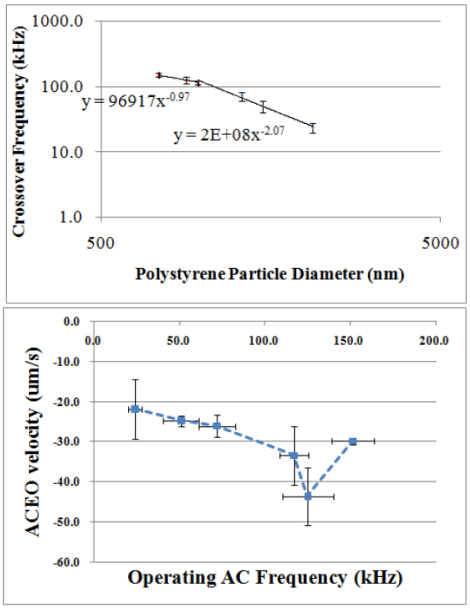

Fig. DEP Crossover frequency as a function of particle size (top) and ACEO velocity as a function of frequency (bottom).

Endothelial cell membrane sensitivity to shear stress is lipid domain dependent: Tristan Tabouillot, Hari S. Muddana and Peter J. Butler (pjbbio@engr.psu.edu) *Penn State University*. Blood flow-associated shear stress causes physiological and pathophysiological biochemical processes in endothelial cells that may be initiated by alterations in plasma membrane lipid domains characterized as liquid-ordered (l_o), such as rafts or caveolae, or liquid-disordered (l_d). To test for domain–dependent shear sensitivity, we used time-correlated single photon counting instrumentation to assess the photophysics and dynamics of the domain-selective lipid analogues DiI-C_{12} and DiI-C_{18} in endothelial cells subjected to physiological fluid shear stress. Under static conditions, DiI-C_{12} fluorescence lifetime was less than DiI-C_{18} lifetime and the diffusion coefficient of DiI-C_{12} was greater than the DiI-C_{18} diffusion coefficient, confirming that DiI-C_{12} probes l_d, a more fluid membrane environment, and DiI-C_{18} probes the l_o phase. Domains probed by DiI-C_{12} exhibited an early (10 s) and transient decrease of fluorescence lifetime after the onset of shear while domains probed by DiI-C_{18} exhibited a delayed decrease of fluorescence lifetime that was sustained for the 2 min the cells were subjected to flow. The diffusion coefficient of DiI-C_{18} increased after shear imposition, while that of DiI-C_{12} remained constant. Determination of the number of molecules (N) in the control volume suggested that DiI-C_{12}-labeled domains increased in N immediately after step-shear, while N for DiI-C_{18}-stained membrane transiently decreased. These results demonstrate that membrane microdomains are differentially sensitive to fluid shear stress.

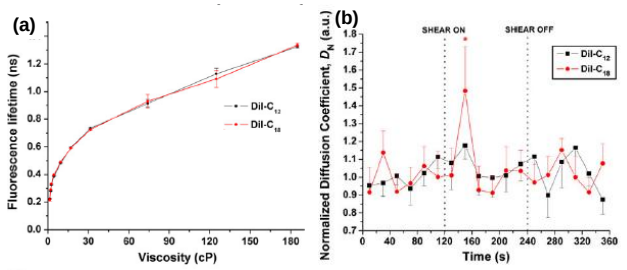

Fig. (a) Assessment of fluorescence lifetime decay mechanisms of DiI. Effects of solution viscosity on fluorescence lifetime (means and standard deviations) of DiI-C12 and DiI-C18. Viscosity was increased by increasing glycerol concentration and was measured in a viscometer. (b)Effects of shear stress on 20-s normalized diffusion coefficient, D, relative to last pre-shear value, for DiI-C12 (n = 7) and DiI-C18 (n = 8). All diffusion coefficients were evaluated using 20-s integration of photon data, were normalized using average of pre-shear values, and are expressed as means and standard errors. Vertical dotted line indicates shear on (or off) time point (* p <0.05).

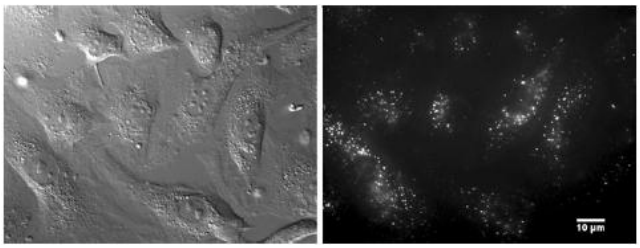

Fig. Glycocalyx staining of BAECs with Alexa Fluor 647-tagged HepSS-1. Staining pattern is similar that reported in Thi.

Substrate catalysis enhances single-enzyme diffusion: Muddana HS, Sengupta S, Mallouk TE, Sen A, and Butler PJ. (pjbbio@engr.psu.edu) *Penn State University*. We show that diffusion of single urease enzyme molecules increases in the presence of urea in a concentration-dependent manner and calculate the force responsible for this increase. Urease diffusion measured using fluorescence correlation spectroscopy increased by 16-28% over buffer controls at urea concentrations ranging from 0.001 to 1 M. This increase was significantly attenuated when urease was inhibited with pyrocatechol, demonstrating that the increase in diffusion was the result of enzyme catalysis of urea. Local molecular pH changes as measured using the pH-dependent fluorescence lifetime of SNARF-1 conjugated to urease were not sufficient to explain the increase in diffusion. Thus, a force generated by self-electrophoresis remains the most plausible explanation. This force, evaluated using Brownian dynamics simulations, was 12 pN per reaction turnover. These measurements demonstrate force generation by a single enzyme molecule and lay the foundation for a further understanding of biological force generation and the development of enzyme-driven nanomotors.

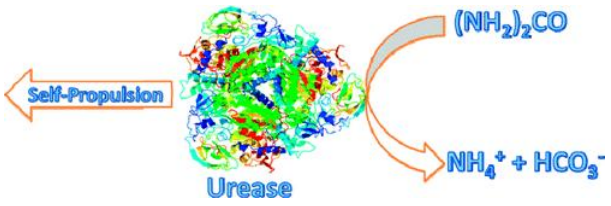

Photophysics of Cy3-encapsulated calcium phosphate nanoparticles: Hari S. Muddana, Thomas T. Morgan, James H. Adair, and Peter J. Butler (pjbbio@engr.psu.edu) *Penn State University*. Progress toward clinical application of biodegradable fluorescent calcium phosphate (CP) nanoparticles as a bioimaging agent requires detailed knowledge of chromophore interaction with CP. As readouts of this cargo-matrix interaction, we determined the principle photophysical properties of Cy3 encapsulated in CP nanparticles (CPNPs) using steady-state and time-resolved fluorescence spectroscopy. Fluorescence correlation spectroscopy (FCS)-determined diffusion coefficients and associated hydrodynamic radii confirmed the presence of highly monodisperse CPNPs with radii ranging from 7 to 10 nm. Single CP nanoparticles were 20 times brighter than free dye molecules because of a CP-induced 5-fold increase in quantum efficiency and encapsulation of four dye molecules per particle. Solvatochromic shifts resulting from hydrogen bonding between free dye and solvent or restricted intramolecular mobility by solvent viscosity were absent when Cy3 was encapsulated in CP. Encapsulation-mediated increases in radiative decay rates and decreases in nonradiative decay rates resulting in longer fluorescence lifetimes of Cy3 were attributed to solvent and CP-related local refractive indices and restricted flexibility of dye by rigid CP. Enhanced brightness of CPNPs enabled imaging of single nanoparticles under epifluorescence using both standard and total internal reflection fluorescence (TIRF) modes with camera exposure times on the order of tens of milliseconds. These enhanced photophysical properties together with excellent biocompatibility make CPNPs ideal for bioimaging applications ranging from single-molecule tracking to in vivo tumor detection and offer the possibility of timed codelivery of drugs to control cell function.

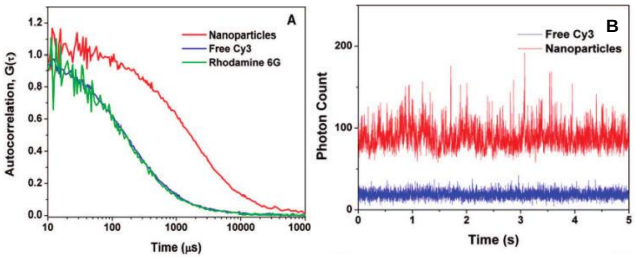

Fig. (A) Normalized autocorrelation of fluorescence fluctuations of CP nanoparticles (red), free Cy3 dye (blue), and rhodamine 6G (green). Shift of the curve to the right signifies smaller diffusion coefficient and larger hydrodynamic radius. (B) Representative raw fluorescence intensity signals from free Cy3 (blue) and CP nanoparticles (red) in PBS. Larger fluorescence fluctuations about the average indicates higher molecular brightness.

Principal Investigators

Filbert J. Bartoli, Lehigh University
Email: fjb205@lehigh.edu

Ivan Biaggio, Lehigh University
Email: ivb2@lehigh.edu

Peter J. Butler, Penn State University
Email: pjbbio@engr.psu.edu

Xuanhong Cheng, Lehigh University
Email: xuc207@lehigh.edu

Volkmar Dierolf, Lehigh University
Email: vod2@lehigh.edu

Sabrina S. Jedlicka , Lehigh University
Email: ssj207@lehigh.edu

H. Daniel Ou-Yang, Lehigh University
Email: hdo0@lehigh.edu

Dimitrios Vavylonis, Lehigh University
Email: vavylonis@lehigh.edu